Dynamics of a thin radial liquid flow

Nicolas De Cock[a,b], Mathieu Massinon[a], Sofyen Ouled Taleb Salah[a], Benoit Mercatoris[a], Maria Rosaria Vetrano[b], Frédéric Lebeau[a]

[a] *University of Liege, Gembloux Agro-Bio Tech, Gembloux 5030, Belgium*
[b] *von Karman Institute, Environmental and Applied Fluid Dynamics Department, 1640 Rhode-Saint-Genèse, Belgium*

Abstract

The present work proposes an extension of the existing analytical development on the radial spread of a liquid jet over a horizontal surface to the case of a thin radial flow. When the gap, H, between the jet nozzle and the plate is reduced the discharging area may be smaller than the inlet area leading to an increase of the main flow velocity downstream of the thin cylindrical opening. This increase of velocity, defined here as $\frac{1}{\alpha}$, can be related to the relative gap of the nozzle $\frac{H}{R}$ with R the nozzle pipe radius. Numerical computations with a volume of fluid method were realised with for $\frac{H}{R}$ ranging from 0.2 to 3 and with flow rates Q of 3 and 6 $l\ min^{-1}$. The results of these computations allowed to express α in respect of $\frac{H}{R}$. Taking in account the flow acceleration allowed to extend the set of equation from the jet impacting flow to the thin cylindrical opening flow. The liquid layer thickness and the surface velocity differ with a maximum error of 4% between the flow predicted by the model and computations. Main discrepancies appear in the region close to the nozzle where the analytical model assumption of a constant velocity outside the boundary layer is not valid. However, further downstream the model and the computations are in good agreement.

Keywords: Liquid sheet formation, CFD, Boundary layer development

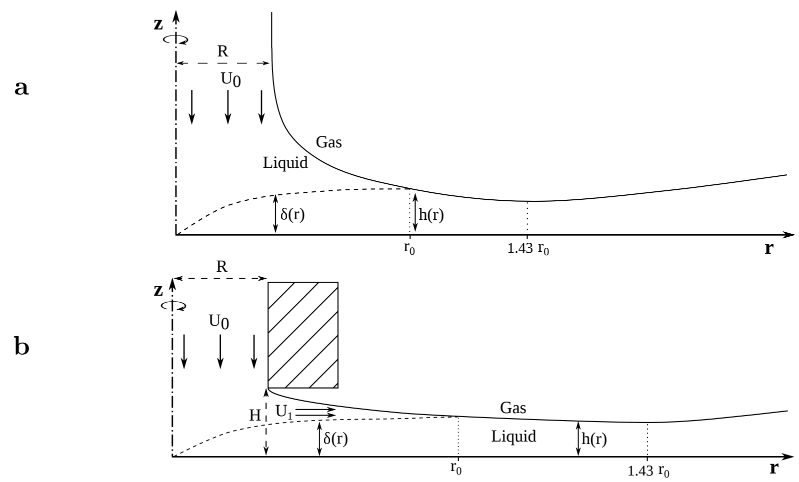

Figure 1: Half radial cut of the radial flow created by a impact of a round jet on a horizontal plate (top) and thin cylindrical opening (bottom). With r the radial distance, R the jet radius, H the distance between the nozzle and the plate, U_0 jet mean velocity, U_1 the main stream velocity, $h(r)$ the liquid film thickness, $U(r)$ the interface velocity and $\delta(r)$ the boundary layer thickness.

1. Introduction

The radial spread of a liquid film created by a round jet impact on a surface (figure 1a) occurs in numerous applications including mass and heat transfer. Surface cooling using an impinging water jet has been studied [1], [2] and [3]. Spray formation by fire sprinkler [4, 5, 6] or plate nozzle [7, 8, 9] involves a liquid film as the first step of a spray formation. The governing parameters of the spray formation process are the thickness and the velocity of the liquid layer. [5] proposed a sprinkler spray model which combines a film flow dynamic model based on analytical solution of [10] with an atomization model. Since sprinkler are usually pressure based, one way to reduce the flow rate whilst keeping the same velocity is is to constraint the liquid by bringing the nozzle closer to the plate (figure 1b). This way of working has the advantage that it does not require

*Corresponding author
Email address: nicolas.decock@ulg.ac.be (Nicolas De Cock)

the modification of the orifice size.

The hydrodynamics of the impact of an axisymmetric liquid jet on a normal surface has been theoretically studied by Watson [10] who provided an analytical solution of the liquid layer thickness $h(r)$ and surface velocity $U(r)$ in respect with the radial distance from the jet centre r, the liquid kinematic viscosity ν, the jet volumetric flow rate Q and the jet radius R. His solution is realized using a self similarity solution and the momentum integral solutions. He distinguished three main regions in the flow. The first one begins at stagnation point where the boundary layer starts growing and it finishes at $r = r_0$ where the whole flow is within the boundary layer. In the second region, the boundary layer is fully developed. The liquid layer thickness is controlled by both radial dispersion and viscous wall effects. The liquid layer thickness is decreasing until $r = 1.43\ r_0$ and then it increases.

Measurements of the liquid layer thickness and the velocity profile realized by Azuma and al [11, 12, 13] using needle probe and laser Doppler velocimeter show a good agreement with the solution proposed by Watson for flows with a Reynolds number ranging from $2.2\ 10^4$ [12] to $1.7\ 10^5$ [13]. The laminar to turbulent transition defined by [11] as the presence of sandpaper-like waves in more than 50 % of the peripheral direction. This transition occurs for a Re around $5\ 10^4$.

When the nozzle is close to the plate (figure 1b), the water is discharging through a thin cylindrical opening creating a thin liquid layer spreading radially. At the inner corner of the constriction, the flow is separating leading to an actual discharging area smaller than $2\pi\, R\, H$. [14] performed 2D numerical computations using the free-streamline theory on right-angle elbows with geometrical ratio, upstream to downstream channel width, ranging from 0.01 to 1.2. They compute the contraction coefficient (C_c) defined as the ratio of the asymptotic stream width downstream of the corner to the upstream channel width. The C_c was decreasing with the geometrical ratio. [15] investigated the effect of the elbow angle on the contraction coefficient showing that C_c was decreasing with the elbow angle. Their computations of the C_c has been validated by [16] who solved the Euler equations of the flow at a corner using a Lagrangian model based on smoothed particle hydrodynamics method.

The goal of this paper is to provide an analytical description of the thickness and the velocity of a thin liquid layer generated by radial flow generated by a thin cylindrical opening. The solution combines the analytical solution given by Watson and a correlation expression the flow acceleration due to the flow separation in respect with the geometrical ratio. The paper is structured as follows: in § 2.1 the theoretical development proposed by Watson for a round jet spreading radially is summarized. The full description of the theoretical developments can be found in Watson's paper [10]; in § 2.2 presents the theoretical extension to a radial flow of the Watson solution; in § 3 presents the numerical computations used to find the relationship between the geometrical ratio and the flow acceleration; finally, in § 4 the validity and the quality of the proposed model is discussed.

2. Theoretical developments

2.1. Flow created by a round liquid jet impacting on a horizontal plate

2.1.1. Fully developed region: similarity solution

This axisymmetric flow can be described as a thin layer by the following equations:

$$\frac{\partial(ru)}{\partial r} + \frac{\partial(rw)}{\partial z} = 0 \tag{1}$$

$$u\left(\frac{\partial u}{\partial r}\right) + w\left(\frac{\partial u}{\partial z}\right) = \nu\left(\frac{\partial^2 u}{\partial z^2}\right) \tag{2}$$

where r is the radial distance from the jet center, z is the distance upward from the plate, u and w are the corresponding velocity components, ν is the kinematic viscosity.

The hypothesis are: a no slip condition at the plate (eq. 3), the shear stress at the free surface is negligible (eq. 4) and the flow rate along the radial axis is constant (eq. 5).

$$u = w = 0 \quad \text{at} \quad z = 0 \tag{3}$$

$$\frac{\partial u}{\partial z} = 0 \quad \text{on} \quad z = h(r) \tag{4}$$

$$Q = 2\pi r \int_0^{h(r)} u \, \mathrm{d}z \tag{5}$$

The velocity profile in the axial direction u can be rewritten as function of the velocity at the free surface $U(r)$ and a similarity solution $f(\eta)$:

$$u = U(r)f(\eta) \quad \text{with} \quad \eta = \frac{z}{h(r)} \tag{6}$$

Then, the flow rate along the radial direction given by the equation 5 can be rewritten as:

$$Q = 2\pi r U h \int_0^1 f(\eta) \, \mathrm{d}\eta \tag{7}$$

Watson used the integral method to retrieve the integral of the velocity profile over the liquid layer thickness equal to:

$$\int_0^1 f(\eta) \, \mathrm{d}\eta = \frac{2\pi}{3\sqrt{3}c^2} \tag{8}$$

with c is a constant of integration equal to 1.402. Finally, the constant flow equation 7 can be rewritten as:

$$rUh = \frac{3\sqrt{3}c^2 Q}{4\pi^2} \tag{9}$$

Using the equations 2 and 9, $U(r)$ and $h(r)$ can be expressed as:

$$U(r) = \frac{27c^2Q^2}{8\pi^4\nu(r^3 + l^3)} \tag{10}$$

$$h(r) = \frac{2\pi^2\nu(r^3 + l^3)}{3\sqrt{3}Qr} \tag{11}$$

where l is a constant length arising from the integration of $\frac{\partial U}{\partial r}$ in the equation 2. The value of l will be determined later using the boundary development region equations knowing that $h(r_0) = \delta$.

2.1.2. Boundary development region: general approximate solution

In the first region, the boundary layer is not fully developed thus the velocity outside the boundary layer is considered as equal to the velocity of the jet U_0 which is expressed as:

$$U_0 = \frac{Q}{\pi R^2} \tag{12}$$

Inside the boundary layer, the velocity profile is defined by the similarity function $f(\eta)$:

$$u = U_0\, f\left(\frac{z}{\delta}\right) \quad \text{with} \quad u = U_0 \quad \text{when} \quad z \geq \delta(r) \tag{13}$$

The momentum integral equation is equal to:

$$\left(\frac{d}{dr} + \frac{1}{r}\right) \int_0^{\delta} (U_0\, u - u^2)\, \mathrm{d}z = \nu \left(\frac{\partial u}{\partial z}\right)_{z=0} \tag{14}$$

Integration and rewriting of equation 14 gives:

$$\delta = \sqrt{\frac{\sqrt{3}c^3 \nu r}{\left(\pi - c\sqrt{3}\right) U_0}} \tag{15}$$

The constant flow rate expression given by equation 5 can be rewritten as:

$$Q = 2\pi r \left(U_0 \delta \int_0^1 f(\eta)\, d\eta + U_0 (h - \delta) \right) \tag{16}$$

From which h can be derived:

$$h(r) = \frac{R^2}{2r} + \left(1 - \frac{2\pi}{3\sqrt{3}c^2}\right) \delta \tag{17}$$

Then, the expression of h is the sum of two effects: the radial dispersion of the flow and the displacement thickness of the boundary layer. This expression is valid until the whole flow is within the boundary layer, *i.e.* when $r \leq r_0$. The r_0 value is determined by founding the location where the boundary layer volume flux is equal to the inlet volume flux:

$$r_0 U_0 \delta(r_0) = \frac{3\sqrt{3}c^2 Q}{4\pi^2} \tag{18}$$

Using equation 15, r_0 is equal to:

$$r_0 = 0.3155 \sqrt[3]{\frac{QR^2}{\nu}} \tag{19}$$

Since U is equal to U_0 when $r = r_0$. Therefore the value of l can be found using equations 9 and 19:

$$l = 0.5673 \sqrt[3]{\frac{QR^2}{\nu}} \tag{20}$$

Finally, the equations describing the liquid layer thickness are equations 17 when $r \leq r_0$ and 11 when $r > r_0$. The surface velocity is equal to the initial velocity U_0 when $r \leq r_0$ and then it is given by the equation 10 when $r > r_0$.

2.2. Radial flow of a thin liquid film

When the gap, H, between the jet nozzle and the plate is reducing the discharging area may be smaller than the inlet area leading to an increase of the main flow velocity downstream of the thin cylindrical opening (figure 1b). Moreover, a flow separation is occurring at the nozzle inner corner leading to the contraction of the streamline which consequently decrease the actual discharging area. The main flow velocity changes from U_0 in the inlet pipe to U_1 downstream of the jet impact region. This increase of velocity is defined here as $\frac{1}{\alpha}$. Therefore, U_1 reads as:

$$\alpha = \frac{U_0}{U_1} = \frac{2HC_C}{R} \tag{21}$$

$$U_1\alpha = U_0 \tag{22}$$

The expression of α should lies between 0 and 1 and it should depends on $\frac{H}{R}$, defined as the opening ratio. Making the hypothesis that the downstream flow can be described by the Watson's model taking in account this main flow acceleration, the height and the surface velocity of the liquid layer can be rewritten adding the new variable α. When $r \leq r_0$, the equations 15, 17 and 20 become:

$$\delta = \sqrt{\frac{\alpha\sqrt{3}c^3\nu r}{(\pi - c\sqrt{3})U_0}} \tag{23}$$

$$h(r) = \frac{\alpha R^2}{2r} + \left(1 - \frac{2\pi}{3\sqrt{3}c^2}\right)\delta \tag{24}$$

$$r_0 = 0.3155\sqrt[3]{\frac{\alpha Q R^2}{\nu}} \tag{25}$$

When $r > r_0$, the equations 10, 11 and 20 become:

$$U(r) = \frac{27c^2Q^2}{8\pi^4\nu(r^3 + l^3)} \tag{26}$$

$$h(r) = \frac{2\pi^2\nu(r^3 + l^3)}{3\sqrt{3}Qr} \tag{27}$$

$$l = 0.5673\sqrt[3]{\frac{\alpha Q R^2}{\nu}} \tag{28}$$

In this set of equation only l is affected by the velocity increase of the main flow.

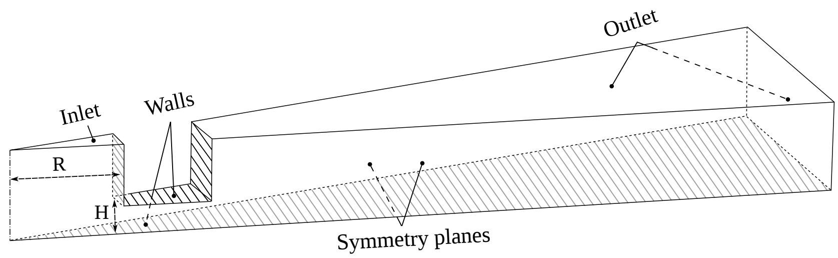

Figure 2: Computational domain used to simulate the flow generated by a thin cylindrical opening with the associated boundary conditions.

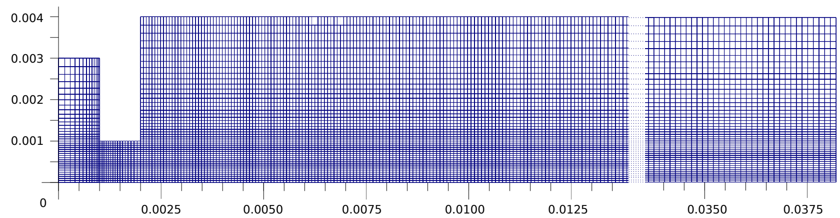

Figure 3: Example of mesh for a nozzle with a radius of 1 mm and a height of 1 mm. The dimensions are given in meters.

3. Numerical modelling

3.1. Computational domain

Since the flow generated by a thin cylindrical opening is axisymmetric, the computational domain was two-dimensional (figure 2). In the radial direction, the domain was starting at the middle of the inlet pipe and it was ending at $r = 3.5\, r_0$. The height of the domain at the top of the plate was set at four time the inlet radius and the height of the inlet was set at three times the inlet radius.

The computational grid was a wedge (figure 2) with an opening angle of $5°$ and 1 cell thick running along the plane of symmetry. The mesh resolution was adapted to each geometry using an automatic routine. A mesh refinement region was set at the exit of the inlet. In this region, the z resolution was set as $\Delta z = min\left(\frac{H}{25}, \frac{R}{75}\right)$ and the r resolution is set as $\Delta r = \frac{R}{15}$. The cell size was growing with the distance from the inlet centre. The maximal cell aspect ratio was 5 and the cell-to-cell expansion ratio was no exceeding 1.1. The number of cells was ranging from 50 000 to 250 000 for the largest geometry. An example of mesh is illustrated by the figure 3.

3.2. Computational parameters

Numerical simulations were performed in order to retrieve the value of α. The effect of the relative gap on the flow acceleration were studied for relative opening ranging from 0.2 to 3. Two different inlet radius R were tested 1 and 2 mm and two flow rates Q: 3 and 6 $l\ min^{-1}$. The Reynolds numbers in the inlet pipe , $Re = \frac{Q}{R\nu}$, were ranging from to 2.5 10^4 to 10^5. The thickness of the inlet pipe wall was 1mm defining the length of the restriction. The fluids used for the simulations were water and air at $20°C$ with the following properties: $\rho_{water} = 998\ kg^1\, m^{-3}$, $\nu_{water} = 1\ 10^{-6}\, m^2 s^{-1}$, $\rho_{air} = 1.2\ kg^1\, m^{-3}$ and $\nu_{air} = 15\ 10^{-6}\, m^2 s^{-1}$. The surface tension effects were neglected.

3.3. Boundary conditions

The inlet boundary was set with an uniform velocity equal to $U_0 = \frac{Q}{\pi R^2}$, a normal gradient of pressure equal to 0 and a liquid fraction ϕ equal to 1. The wall boundaries were set as no slip, zero normal gradients for ϕ and the pressure. The outlet was set at atmospheric pressure with no liquid backflow. Axisymmetric boundary conditions were set the for the front and back plans of the domain.

3.4. Numerical method

The InterFoam solver from the *OpenFOAM C++* toolbox has been used to perform numerical simulations. InterFoam is a Volume Of Fluid (VOF) solver for incompressible two-phase flow. This solver provided good results for inertia-dominated flows with large fluid density ratios ($\geq 10^3$), such as round jet impact [17]. The governing equations are discretised and solved using the finite volume method and the PISO algorithm respectively. The diffusion terms were discretized using a second order central difference scheme. All the cases were considered in a laminar mode since the range of simulation is close or below the laminar to turbulence transition [12]. Therefore, no extra turbulence model has been used. The computations were unsteady and the time step was controlled by the Courant number set at 0.45. Consequently, the results presented in the next section are an averaged solution of the flow over a certain time interval at the steady state.

3.5. Post processing

The liquid layer thickness $h(r)$ was computed by integrating the liquid fraction ϕ over the z direction: $h(r) = \int \phi(r)\,\mathrm{d}z$. The surface velocity was computed at the location where $\phi = 0.5$ using a linear interpolation. In order to present results in a concise way, the radial distance, the height and the surface velocity profiles are expressed in non dimensional way: $r^* = r\sqrt[3]{\frac{\nu}{\alpha Q R^2}}$, $h^* = h(r)\sqrt[3]{\frac{Q}{\alpha^2 \nu R^4}}$ and $U^* = 10\left(\frac{\alpha U(r)}{U_0}\right)$.

α_{obs} was computed using the equation 21. U_1 was computed as the average of the main flow velocity from $r = 0$ until $r = r_0$. Moreover, three extra values of α were computed by fitting. The liquid sheet thickness equations 24 and 27 were reduced to two simpler expressions depending on the radial distance r and on four coefficients a, b, d and e. For each case, the values of the four coefficients were retrieved by fitting the equation 29 on the thickness profile $h(r)$ from the numerical data.

$$h(r) = \begin{cases} \frac{a}{r} + b\sqrt{r}, & r \leq r_0 \\ \frac{d\left(r^3+e\right)}{r}, & r > r_0. \end{cases} \tag{29}$$

Then, from the equations 23, 24 and 28, three expressions of α were obtained:

$$\begin{cases} \alpha_a = \frac{2\,a}{R^2} \\ \alpha_b = \left(\frac{b\,\sqrt{U_0}}{0.9955\,\sqrt{\nu}}\right)^2 \\ \alpha_e = \frac{e\,\nu}{0.1826\,Q\,R^2} \end{cases} \tag{30}$$

There is no expression for α_d since d is independent of α. Finally, some flow acceleration for similar flow available in the literature are used for comparison.

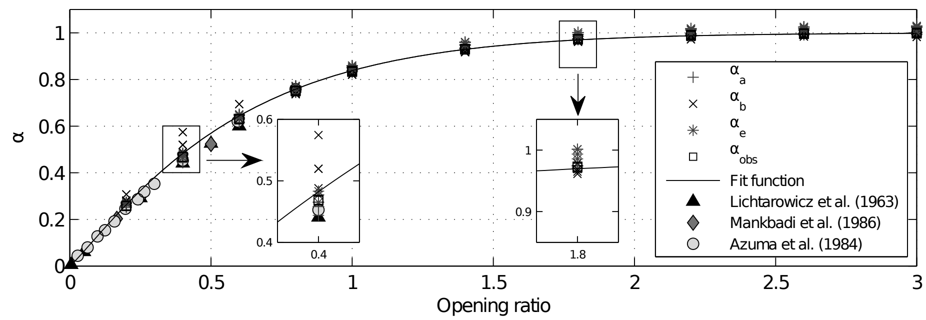

Figure 4: Comparison of the value of α retrieved from the post processing or found in the literature in respect with the relative gap.

[14] and [18] computed the contraction coefficient for a 90° elbow with several ratios upstream to downstream. [11] realized measurements of the flow velocity at the exit of a circular inlet for small opening ratios.

3.6. Model quality

The quality of the analytical model given by the equations 24 and 27 was assessed by computing the Normalised Root Mean Square Deviation (NRMSD) using the numerical data as observed values. The NRMSD was computed as:

$$NRMSD = \frac{\sqrt{\frac{1}{n}\sum_{i=1}^{n}\left(\hat{Y}_i - Y_i\right)^2}}{(Y_{max} - Y_{min})} \tag{31}$$

where n is the number of observation, $\hat{Y}_i$ are the values predicted by the model, Y_i are the observed values and $(Y_{max} - Y_{min})$ is the amplitude of the variation within the dataset.

4. Results and discussion

Comparison of the different α in respect with the relative gap is presented on the figure 4. α is increasing with the opening ratio until the asymptotic value of 1 is reached. For most of the cases the different values of α are close to each other. Therefore, taking in account the flow acceleration allows to extend the

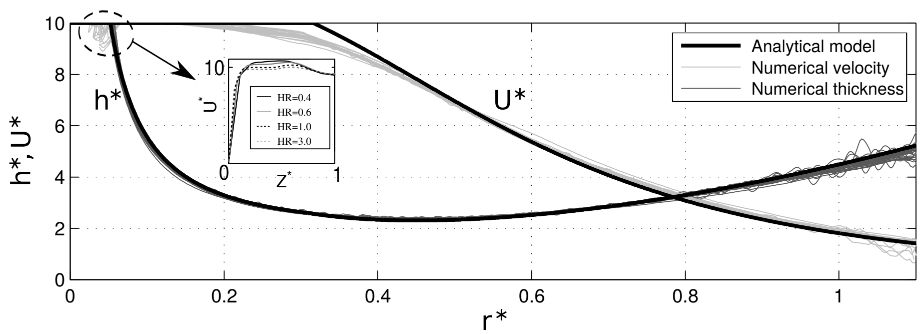

Figure 5: Comparison between between the numerical data from all the cases and the model prediction for the surface velocity and liquid thickness in respect with the radial distance. The inside graph gives the velocity profiles close at 1 mm from the nozzle exit for the cases with $R = 1\ mm$ and $H = 0.4$, 0.6, 1 and 3 mm with $z^* = \frac{z}{\delta}$.

set of equation from the jet flow to the thin cylindrical opening flow. When the opening ratio is small, i. e. < 1.5, there are discrepancies between the different values of α and α_b. α_b is larger than the other values of α showing that the displacement thickness induced by the boundary layer development is larger than expected. For these cases, close to the inlet the velocity outside boundary layer is not equal to the free stream velocity everywhere. Indeed, the velocity is lower close to the liquid/air interface. Therefore, the liquid height is higher than expected to compensate this deficit of velocity. When the opening ratio is large, i.e. > 1.5, α is close to one, therefore the flow is close to the free jet impact flow. The comparisons with the measurements of [11] show good agreement as well as the theoretical contraction coefficients computed by [14] and [18]. From these results, α can be expressed in respect with the opening ratio $\frac{H}{R}$ as:

$$\alpha = \left(1 - e^{-1.82\left(\frac{H}{R}\right)^{1.11}}\right) \tag{32}$$

The figure 5 compares the numerical data from all the cases and the model prediction for the surface velocity and liquid thickness in respect with the radial distance. The reduction to a non dimensional expression of $U(r)$ and $h(r)$ was realized using the expression of α given by the equation 32. After, the reduction to the non dimensional expression all the curves are really close to each other

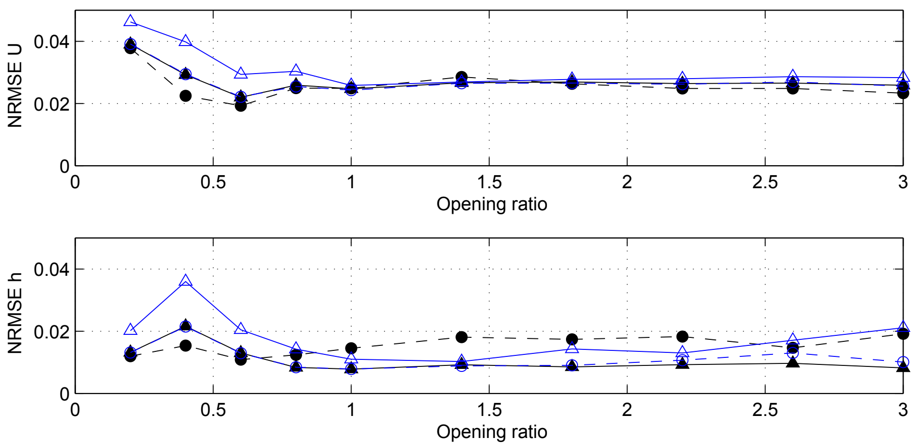

Figure 6: NRMSD on the interface velocity (top) and the liquid sheet thickness (bottom) predictions in respect with the relative opening ratio. Each marker corresponds to a specific radius/flow rate combination: - -△- - is for $R = 1\ mm$ & $Q = 3\ l\ min^{-1}$, —○— is for $R = 2\ mm$ & $Q = 6\ l\ min^{-1}$,—▲— is for is for $R = 2\ mm$ & $Q = 3\ l\ min^{-1}$ and - -●- - is for $R = 2\ mm$ & $Q = 6\ l\ min^{-1}$.

showing that the flow equations with α are describing on the downstream flow well the effect of the gap between the inlet and the plate. When $r^* < 0.1$, the surface velocity is lower than the main stream velocity as illustrated by the inside graph. When $0.3 < r^* < 0.4$, the observed values are lower than the predicted one because the velocity profile was decreasing close to the interface liquid/air. For the liquid layer thickness $h(r)$, the prediction and the observed data are really close to each other. For r^* close to 1, some numerical instabilities are observed for both simulations creating wiggles in the solutions.

The NRMSD on the liquid sheet thickness and interface velocity prediction in respect with the relative opening ratio are presented on the figure 6. For both the surface height and the surface velocity, the NRMSD is larger when the opening ratio is smaller than 1. Then, when the opening ratio is larger than 1 the NRMSD is equal to 3 % for the surface velocity and to 2 % for the liquid layer thickness. There is no significative difference between the different cases.

5. Conclusion

The present work proposed an extension of the existing analytical development on the radial spread of a liquid jet over a horizontal surface to the case of a laminar thin radial flow. When the gap, H, between the jet nozzle and the plate is reduced the discharging area may be smaller than the inlet area leading to an increase of the main flow velocity downstream of the thin cylindrical opening. This increase of velocity, defined here as $\frac{1}{\alpha}$, can be related to the relative gap of the nozzle $\frac{H}{R}$. Numerical computations with a volume of fluid method were realised for $\frac{H}{R}$ ranging from 0.2 to 3 and with Q of 3 and 6 $l\ min^{-1}$. The results of these computations allowed to express α in respect of $\frac{H}{R}$. α is increasing with the opening ratio until the asymptotic value of 1 is reached. Taking in account the flow acceleration allowed to extend the set of equation from the jet impacting flow to the thin cylindrical opening flow. The liquid layer thickness and the surface velocity differ with a maximum error of 4 % between the flow predicted by the model and computations. Main discrepancies appear in the region close to the nozzle where the analytical model assumption of a constant velocity outside the boundary layer is not valid. However, further downstream the model and the computations are in good agreement. The present analytical model and correlation has been done for laminar flow ($Re < 10^5$). The extension of this model to turbulent flow would required to take in account the extra mixing induced by the eddies and it may also require to adapt the velocity profile. Further work will focus on the experimental validation of the proposed analytical solution.

6. Acknowledgements

This work was supported by the Belgian Industrial and Agricultural Research Funds (FRIA) [grant number 26325996]. Computational resources have been provided by the Consortium des quipements de Calcul Intensif (CCI), funded by the Fonds de la Recherche Scientifique de Belgique (F.R.S.-FNRS) under Grant No. 2.5020.11.

References

[1] S. Ishigai, S. Nakanishi, M. Mizuno, T. Imamura, Heat transfer of the impinging round water jet in the interference zone of film flow along the wall, Bulletin of JSME 20 (139) (1977) 85–92.

[2] X. Liu, J. H. Lienhard, J. S. Lombara, Convective heat transfer by impingement of circular liquid jets, Journal of heat transfer 113 (3) (1991) 571–582.

[3] M. L. Hosain, R. B. Fdhila, A. Daneryd, Heat transfer by liquid jets impinging on a hot flat surface, Applied Energy 164 (2016) 934–943.

[4] A. W. Marshall, M. Di Marzo, Modelling aspects of sprinkler spray dynamics in fires, Process Safety and Environmental Protection 82 (2) (2004) 97–104.

[5] D. Wu, D. Guillemin, A. W. Marshall, A modeling basis for predicting the initial sprinkler spray, Fire safety journal 42 (4) (2007) 283–294.

[6] H. Aghajani, S. Dembele, J. X. Wen, Analysis of a semi-empirical sprinkler spray model, Fire Safety Journal 64 (2014) 1–11.

[7] N. De Cock, M. Massinon, B. C. N. Mercatoris, F. Lebeau, Numerical modelling of mirror nozzle flow, in: Montreal, July 13 – July 16, 2014, ASABE, 2014, pp. 3632–3640.

[8] M. P. Fard, D. Levesque, S. Morrison, N. Ashgriz, Characterization of splash-plate atomizers using numerical simulations, Atomization and Sprays 17 (4) (2007) 347–380.

[9] J. M. Gordillo, H. Lhuissier, E. Villermaux, On the cusps bordering liquid sheets, Journal of Fluid Mechanics 754 (2014) R1.

[10] E. J. Watson, The radial spread of a liquid jet over a horizontal plane, Journal of Fluid Mechanics 20 (3) (1964) 481–499.

[11] T. Azuma, T. Hoshino, The radial flow of a thin liquid film: 1^{st} report, laminar-turbulent transition, Bulletin of JSME 27 (234) (1984) 2739–2746.

[12] T. Azuma, T. Hoshino, The radial flow of a thin liquid film: 2^{nd} report, liquid film thickness, Bulletin of JSME 27 (234) (1984) 2747–2754.

[13] T. Azuma, T. Hoshino, The radial flow of a thin liquid film: 3^{rd} report, velocity profile, Bulletin of JSME 27 (234) (1984) 2755–2762.

[14] A. Lichtarowicz, E. Markland, Calculation of potential flow with separation in a right-angled elbow with unequal branches, Journal of Fluid Mechanics 17 (4) (1963) 596–606.

[15] S. S. Chu, Separated flow in bends of arbitrary turning angles, using the hodograph method and kirchhoffs free streamline theory, Journal of fluids engineering 125 (3) (2003) 438–442.

[16] Q. Hou, A. C. H. Kruisbrink, F. R. Pearce, A. S. Tijsseling, T. Yue, Smoothed particle hydrodynamics simulations of flow separation at bends, Computers and Fluids 90 (2014) 138–146.

[17] S. S. Deshpande, L. Anumolu, M. F. Trujillo, Evaluating the performance of the two-phase flow solver interfoam, Computational Science and Discovery 5 (1).

[18] R. Mankbadi, S. Zaki, Computations of the contract coefficient of unsymmetrical bends, AIAA journal 24 (8) (1986) 1285–1289.